JOURNAL OF GEOPHYSICAL RESEARCH: OCEANS, VOL. 118, 1–12, doi:10.1002/jgrc.20294, 2013

Revisiting internal waves and mixing in the Arctic Ocean

John D. Guthrie,[1] James H. Morison,[1] and Ilker Fer[2]

Received 11 February 2013; revised 14 June 2013; accepted 27 June 2013.

[1] To determine whether deep background mixing has increased with the diminishment of the Arctic sea ice, we compare recent internal wave energy and mixing observations with historical measurements. Since 2007, the North Pole Environmental Observatory has launched expendable current probes (XCPs) as a part of annual airborne hydrographic surveys in the central Arctic Ocean. Mixing in the upper 500 m is estimated from XCP shear variance and Conductivity-Temperature-Depth (CTD) derived Brunt-Väisälä frequency. Internal wave energy levels vary by an order of magnitude between surveys, although all surveys are less energetic and show more vertical modes than typical midlatitude Garrett-Munk (GM) model spectra. Survey-averaged mixing estimates also vary by an order of magnitude among recent surveys. Comparisons between modern and historical data, reanalyzed in identical fashion, reveal no trend evident over the 30 year period in spite of drastic diminution of the sea ice. Turbulent heat fluxes are consistent with recent double-diffusive estimates. Both mixing and internal wave energy in the Beaufort Sea are lower when compared to both the central and eastern Arctic Ocean, and expanding the analysis to mooring data from the Beaufort Sea reveals little change in that area compared to historical results from Arctic Internal Wave Experiment. We hypothesize that internal wave energy remains lowest in the Beaufort Sea in spite of dramatic declines in sea ice there, because increased stratification amplifies the negative effect of boundary layer dissipation on internal wave energy.

Citation: Guthrie, J. D., J. H. Morison, and I. Fer (2013), Revisiting internal waves and mixing in the Arctic Ocean, *J. Geophys. Res. Oceans*, *118*, doi:10.1002/jgrc.20294.

1. Introduction

[2] Internal waves and their associated mixing are critical to the circulation and thermodynamics of the Arctic Ocean. Warm, saline water from the Atlantic enters the Arctic Ocean through Fram Strait where it circulates cyclonically and topographically steered around the basin. In the Nansen and Amundsen basins, this Atlantic Water (AW) is overlain by the cold halocline (CHL), a region of strong stratification, e.g., the buoyancy frequency $N^2 = 10^{-4}$ s^{-1}, which prevents interaction of the ice cover with AW heat by direct surface-generated mixing. Only dissipation of internal wave energy or double diffusive phenomena can mix fresh water down and AW heat up toward the mixed layer and the ice. The AW further deepens as it circulates into the Canada Basin, where it is overlain by Pacific-derived water with its own temperature maximum. Here again, the haline stratification dictates that vertical mixing is dependent on internal wave dissipation. Some studies have shown the cold halocline weakening in recent years [*Steele and Boyd*, 1998]. Other studies have shown that even modest heat fluxes, 2–7 W m^{-2}, can have significant and irreversible effects on the sea ice concentration [*Maykut and Untersteiner*, 1971; *Polyakov et al*., 2011].

[3] A modeling study [*Zhang and Steele*, 2007] has shown the sensitivity of the Arctic Ocean to background diapycnal diffusivity. Using the *K*-profile parameterization [*Large et al*., 1994], *Zhang and Steele* [2007] found the background diffusivity that produced water properties and circulation that agreed best with the Polar Science Center Hydrographic Climatology [*Steele et al*., 2001] of the Arctic Ocean was 10^{-6} m^2 s^{-1}. This is much less than the 10^{-4} m^2 s^{-1} abyssal mixing rate suggested by Walter Munk [*Munk*, 1966; *Munk and Wunsch*, 1998] and the 10^{-5} m^2 s^{-1} value found in most open ocean models [e.g., *Large et al*., 1994]. *Zhang and Steele* [2007] found that such large values excessively weakened modeled stratification in the Canada Basin, leading to an erosion of the cold halocline and reversing the cyclonic circulation of the Atlantic Water.

[4] In the deep ocean, stratification limits the penetration of turbulence generated at the surface and mixing comes from the dissipation of internal waves, which propagate freely in the stratified region. This, and in some cases double diffusion, are responsible for the vertical fluxes of heat, salt, and momentum in the deep ocean. Consequently,

[1]Polar Science Center, Applied Physics Laboratory, University of Washington, Seattle, Washington, USA.
[2]Geophysical Institute, University of Bergen, Bergen, Norway.

Corresponding author: J. D. Guthrie, Polar Science Center, Applied Physics Laboratory, University of Washington, 1013 NE 40th St., Seattle, WA 98105, USA. (guthriej@apl.washington.edu)

2169-9275/13/10.1002/jgrc.20294

methods have been developed to estimate turbulent dissipation and mixing at microscales from measurements of internal wave energy at fine scale with assumptions about the energy cascade through the internal wave spectrum [*Gregg*, 1989]. The *Zhang and Steele* [2007] result is consistent with observations in the 1980s of low internal wave energies made with expendable current profilers (XCPs) and background mixing (as low as 10^{-6} m^2 s^{-1} in the abyssal Arctic Ocean) derived using the *Gregg* [1989] parameterization [*D'Asaro and Morison*, 1992]. A section of temperature microstructure measurements across the Arctic Ocean in 2005 [*Rainville and Winsor*, 2008] also found low levels of mixing consistent with *D'Asaro and Morison* [1992].

[5] A number of explanations have been offered for these low energy levels and mixing rates in the Arctic Ocean. One includes weak tidal forcing and the fact that most of the basin is north of the critical latitude of the M_2 tide, limiting the spread of internal wave energy generated by the interaction of barotropic tides with bathymetry [*Simmons et al*., 2004; *St. Laurent et al*., 2002]. With the exception of the Yermak Plateau, the results of *Simmons et al*. [2004] indicate that although locally important, internal tide energies in the Arctic Ocean are low compared to typical low-latitude levels. The low internal tide energy levels highlight the importance of atmospheric forcing as the major energy input into the internal wave field of the deep Arctic Ocean. However, the sea ice cover also reduces internal wave energy production [*Levine et al*., 1985, 1987]. Near-inertial internal waves, those slightly above the inertial frequency, dominate the energetics of the internal wave field [*Garrett and Munk*, 1972, 1975]. They are forced by wind-generated near-inertial motion at the surface. Wind-driven near-inertial motion of the ice tends to be limited in solid winter ice conditions but is more common in summer when the ice pack is relatively loose [*McPhee*, 2008; *Plueddemann et al*., 1998; *Rainville and Woodgate*, 2009]. However, there have been indications of enhanced near-inertial motion in winter [*Merrifield and Pinkel*, 1996] and in early winter after freeze up [*Halle and Pinkel*, 2003]

[6] Internal wave energy in the Arctic Ocean is reduced by energy dissipation in the under-ice, surface boundary layer [*Morison et al*., 1985]. acoustic Doppler current profiler velocity measurements during the 1997–1998 SHEBA (Surface Heat Balance of the Arctic Ocean) drift [*Pinkel*, 2005] show that under-ice dissipation is likely a dominant mechanism of internal wave energy loss. *Pinkel* [2005] postulates that with a reduced ice cover, the near-inertial waves would propagate farther and energy, especially that delivered to the basin boundaries, might be greatly increased [*Rainville and Woodgate*, 2009].

[7] Annual minimum sea ice extent [*Stroeve et al*., 2007] and thickness [*Kwok et al*., 2009; *Rothrock et al*., 2008] have decreased about 40% since the early 1980s when the *D'Asaro and Morison* [1992] observations were made. The declines have continued with ice extent reaching a new minimum in 2012. Given that we think sea ice reduces internal wave energy, we ask whether internal wave energy and mixing in the Arctic basin have increased with the areal reduction and thinning of the ice cover? We address this question by comparing the observations of the 1980s with the same types of measurements made in the last few years.

2. Methods

[8] We compare recent observations of internal waves and mixing with the observations analyzed by *D'Asaro and Morison* [1992] using the *Gregg* [1989] formulation. However, since that time the derivation of mixing from internal wave measurements has been improved to account for the influence of latitude on the internal wave environment [*Gregg et al*., 2003] and departures of internal wave spectra from the Garrett-Munk [*Garrett and Munk*, 1975] (GM) form [*Polzin et al*., 1995]. Consequently, we have analyzed both the recent and historical velocity and density profile data following a method [*Kunze et al*., 2006] that incorporates these improvements to estimate internal wave energy, dissipation, and the deep background mixing coefficient, K. To account for the low energy environment of the Arctic Ocean and the limited depth range of our CTD data, our results are confined to the portion of the water column, 150–400 m, containing the cold halocline and extending down past the temperature maximum in the AW. This also allows us to examine the heat flux from the AW to the CHL while avoiding contamination from XCP surface noise and erroneously high diffusivities due to surface mixing and noise-dominated low stratification.

[9] Velocity profiles were WKB stretched by buoyancy frequency [*Leaman and Sanford*, 1975] and tapered using a 10% Tukey window before spectral analysis was performed. Different window choices provided consistent results in terms of power spectral density for the wave number ranges analyzed. Individual spectra were then averaged to create one spectrum per survey. No averaging among frequency bands was done. All horizontal velocity spectra were calculated from U and V velocity as $\Phi_U + \Phi_V \cong \Phi_{CW} + \Phi_{CCW}$, where Φ_U and Φ_V represent U and V velocity spectra, and Φ_{CW} and Φ_{CCW} are the clockwise (CW) and counterclockwise (CCW) rotary spectra [*Gonella*, 1972].

[10] GM fits to the horizontal kinetic energy (HKE) spectra are calculated as in *D'Asaro and Morehead* [1991]. Horizontal velocity spectra were divided by two to turn them into HKE spectra. Fits were then made with the GM "dropped" HKE spectra, retaining cutoff mode number, j_*, and energy, E_0, as free parameters. These are then fit to the data and compared with typical midlatitude values. In *Garrett and Munk* [1975], the horizontal kinetic energy spectrum, $E(\beta)$ is calculated as

$$E(\beta) = \left[N_0^2 b^3\right]\left[\frac{3E_0}{2j_*\pi}\right]\frac{(t-1)}{(1+\lambda)^t} \tag{1}$$

where

$$\lambda = \frac{\beta}{j_*\pi f} \tag{2}$$

[11] Standard values used include $b = 1300$ m, the scale depth of the thermocline; $t = -2.5$, the spectral slope; N_0 is the reference buoyancy frequency, 3 cycles/h; and β is the vertical wave number (units are in m^{-1}). Typical midlatitude values for the model are $j_* = 6$ and $E_0 = 6.3 \times 10^{-5}$.

[12] Based on theories of nonlinear wave-wave interactions and downscale energy transfer in the Garrett-Munk model, the fine-scale shear parameterization used to

estimate K and ε is based on the most recent iteration from *Kunze et al*. [2006].

$$K = K_0 \frac{\langle V_z^2 \rangle^2}{\langle V_z^2 \rangle_{GM}^2} h_1(R_\omega) L(f,N) \tag{3}$$

$$h_1(R_\omega) = \frac{3}{2\sqrt{2}} \frac{R_\omega + 1}{R_\omega \sqrt{R_\omega - 1}} \tag{4}$$

$$L(f,N) = \frac{f \cosh^{-1}(N/f)}{f_{30} \cosh^{-1}(N_0/f_{30})} \tag{5}$$

[13] Here K_0 is 5×10^{-6} m^2 s^{-1}, the diffusivity calculated from GM internal wave shear. R_ω represents the shear to strain variance ratio, an estimate of the ratio between horizontal kinetic energy to available potential energy, which accounts for departures from GM. $L(f,N)$ represents the latitudinal variation in ε [*Gregg et al*., 2003], where f_{30} is the Coriolis frequency at 30° latitude, the reference latitude in GM.

[14] Shear and strain for XCP data were calculated using spectral analysis of 64 m overlapping profile segments of 1 m data centered every 10 m. Fine-scale shear variance, $\langle V_z^2 \rangle$, was calculated by multiplying $\Phi_U + \Phi_V$ by $(2\pi k_z)^2$. Shear variance was then integrated out to k_c such that $\langle V_z^2 \rangle = 0.7N^2$ and then taking $\langle V_z^2 \rangle^2 / \langle V_z^2 \rangle_{GM}^2 = (0.1/k_c)^2$ where k_c is the cutoff wave number and $0.7N^2$ is the value of $\langle V_z^2 \rangle_{GM}$ integrated out to 0.1 cpm. Experiments with different segment lengths produced consistent results. Strain was calculated as $\xi_z = N^2 - \overline{N^2}/\overline{N^2}$ where $\overline{N^2}$ is estimated by a second-order polynomial fit to the observed N^2 segment. N^2 profiles were calculated from sorted potential density, σ_θ, profiles using the adiabatic leveling method [*Fofonoff*, 1985]. Although sometimes present, thermohaline staircases were not commonly apparent in our profiles. The 2 m resolution of the McLane Moored Profiler (MMP) data and the roughly 1 m resolution of the North Pole Environmental Observatory (NPEO) CTD data smooth the majority of the staircase features. At depths and locations where they do occur, the staircases can introduce noise in the strain and strain calculation, but at scales smaller than the 10 m scale of the strain calculation. In the XCP data, R_ω was calculated as a survey average and a single value was applied to the diffusivity profile, while in the MMP data, it was applied to individual profiles due to the longer time record available. Turbulent heat flux is calculated as $F_H = -\rho C_p K \langle dT/dz \rangle$. Temperature gradient is calculated from survey-averaged temperature profiles for each survey. All recent observations are compared with reanalysis of the 1980s data used in *D'Asaro and Morison* [1992] reprocessed identically to the contemporary data.

3. Data

[15] We use XCP and CTD data from the three programs in the 1980s utilized by *D'Asaro and Morison* [1992]: the 1985 Arctic Internal Wave Experiment (AIWEX), the 1983 Marginal Ice Zone Experiment (MIZEX 83) on the *RV Polarbjorn*, and the 1987 ARKTIS IV/3 cruise of the *RV Polarstern* (Figure 1). These are compared to data from four modern XCP/CTD surveys since 2007 made as part of

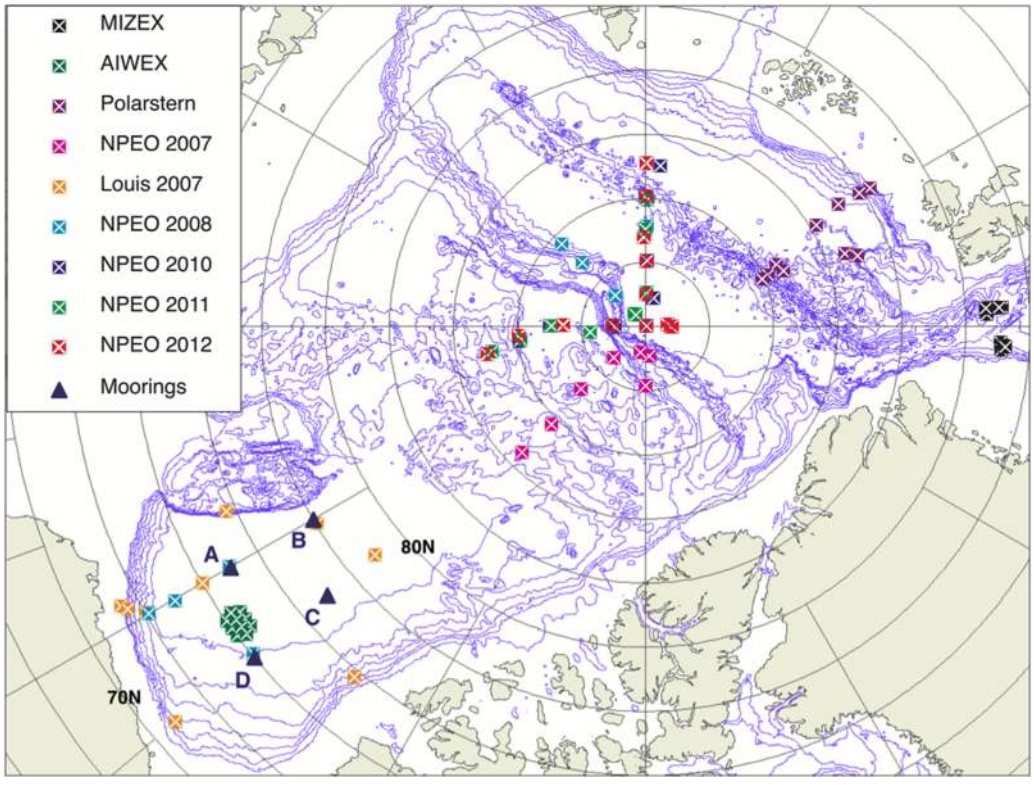

Figure 1. Bathymetric chart of the Arctic Ocean detailing the location of all XCP drops and the BGEP moorings.

the annual NPEO airborne hydrographic surveys (http://psc.apl.washington.edu/northpole/CTDs.html).

[16] Over 40 AIWEX profiles are from the Canada Basin (73°N–74°N, 150°W) between March and April 1985. XCP and CTD data from MIZEX 83 and ARKTIS IV/3 were made mainly between June and July in the eastern Arctic (north of the Yermak Plateau), but some data from ARKTIS IV/3 are from farther north in the Nansen Basin.

[17] NPEO data are from airborne hydrographic surveys mainly in the central Arctic (85°N–90°N) during April, but several stations were made in the Beaufort Sea in March 2008. Water temperature and salinity profiles at these stations are measured to a depth of 900 m with a Sea-Bird 19 or 19+ CTD. In 2007, NPEO XCP drops were also made from the *CGCC Louis St. Laurent* during a Beaufort Gyre Exploration Project (BGEP) cruise in the Canada Basin. CTD data from that cruise are provided by the BGEP (http://www.whoi.edu/page.do?pid=66296).

[18] The XCP (http://www.sippican.com/contentmgr/showdetails.php/id/312) measures currents by measuring the voltage induced by the motion of the conducting seawater through the earth's magnetic field. The probe rotates as it falls, and a flux gate compass is used to resolve probe orientation, and U and V are determined from the induced voltage signal in phase and in quadrature with the direction signal. As the profiler falls, it transmits analog signals through a fine wire to a radio transmitter and recording system at the surface. Depth is given through the known fall rate of the instrument (~3 m/s). The instrument can record velocity down to a depth of 1800 m. Velocity error is calculated during processing based on the variance about a running harmonic fit to the oscillating voltage and heading signals. Velocity error is determined in processing and varies based on goodness of fit but is typically less than 1 cm s^{-1}.

[19] To provide an enhanced view of contemporary conditions in the Beaufort Sea, XCP data are supplemented with time series hydrographic and velocity data from MMPs comprising the BGEP moorings. The MMPs are each equipped with a CTD and a 2-D Acoustic Current Meter made by Falmouth Scientific. The MMP data are available at 2 m resolution on the BGEP website (http://www.whoi.edu/page.do?pid=66559). Estimated velocity errors are 1 cm s^{-1} in magnitude and $\pm 3°$ in direction.

[20] The MMP data were analyzed similarly to the XCP data, except that the spectral analysis was performed over 128 m (64 data point) windows. $\overline{N^2}$ profiles for the MMP data are calculated as monthly averages. MMP diffusivities are split up into spring and summer averages for each year. Spring averages consist of all profiles made during March and April, while summer averages consist of all profiles made during July and August as these are the months that most closely coincide with the XCP data. The monthly average MMP diffusivities show minimal seasonal variability and indicate that these periods are representative. All MMP averages cover the same depth range as XCP data (150–400 m).

[21] For the internal wave analysis, profiles with spikes or large velocity errors throughout the depth range were discarded. As did *D'Asaro and Morison* [1992], we have not included profiles in eddies in our comparisons because the internal wave induced shear is overshadowed by geostrophic shear due to the eddies, the validity of the internal wave-to-mixing formalism is uncertain within the eddy, and fluxes due to background mixing are possibly overshadowed by the ventilation produced by the larger-scale interaction of eddies with their surroundings. However, microstructure measurements made in a cyclonic eddy during AIWEX do show enhanced dissipation [*Padman et al*., 1990]. To check the criticality of excluding eddies in our averages, we have computed the average mixing coefficients for the Beaufort Sea MMP data with and without eddies and find that their inclusion increases average mixing by 10%, well within the confidence limits of the averages. This increase is primarily due to the presence of numerous eddies at mooring A which appears to be a hot spot of eddy activity compared to the other moorings (C. Lique et al., Diffusive vertical heat flux in the Canada Basin of the Arctic Ocean inferred from moored instruments, submitted to *Journal of Geophysical Research: Oceans*, 2013). The presence of heightened mixing over shallow bathymetry is well documented [*D'Asaro and Morison*, 1992; *Padman and Dillon*, 1991]. However, our focus is the mixing in the deep ocean, and our NPEO XCP data and the MMP data are all in the deep basin, so we do not consider comparisons, for example, with the Yermak Plateau profiles of MIZEX 83 and Polarstern 87. Considering deep water only, we are left with ~80 profiles. The number of profiles per survey ranges between 5 from the Louis St. Laurent 2007 cruise and 40 from AIWEX, with most recent surveys consisting of around 7–10 profiles.

4. Validation

[22] The Gregg-Polzin technique approximates the rate of energy dissipation due to wave breaking from the net energy transfer toward smaller scales associated with nonlinear interactions in a slowly varying wave field. This is then related to eddy diffusivity using the *Osborn* [1980] model. The relationship (equation (3)), which depends on the fine scale shear variance squared and the shear-strain ratio (R_ω), has been validated by several field programs in midlatitudes [*Lee et al*., 2006; *Nash et al*., 2007; *Polzin et al*., 1995]. Application of the scaling in low stratification regions may be dominated by noise resulting in spuriously large diffusivities [*Kunze et al*., 2006]. This is not a concern for our results, which are obtained between 150 and 400 m in the stratified part of the water column.

[23] Our method of estimating mixing is tested with a comparison among K parameterized using the original *Gregg* [1989] (G89) and the *Kunze et al*. [2006] (K06) approaches applied to XCP and CTD profiles and calculated from microstructure measurements using an MSS90L, a loosely tethered free-fall profiler made by ISW Wassermesstechnik in Germany. The MSS90L diffusivity profiles are obtained, down to 500 m, from dissipation measurements made with two airfoil shear probes, using the *Osborn* [1980] model. Application of the Osborn model is identical in the fine scale parameterization and the microstructure measurements, each using a mixing efficiency of 0.17. The processing of the microstructure data follows that of *Fer* [2006, 2009]. The noise level in dissipation rate measurements is 5×10^{-10} W kg^{-1}.

[24] Joint microstructure and XCP measurements are available in the marginal ice zone, from a cruise over the Yermak Plateau in 2007, and in the pack ice during the

drifts of the NPEO base camp near the North Pole in 2007 and 2008. The profile pairs collected in Yermak 2007 and NPEO 2008 are within 1 h and 1 km separation. Those collected in NPEO 2007 however are separated by 0.5–2.7 km and 2–10 h. In total, high quality data from 31 profile pairs were recovered (4 from NPEO 2007, 18 from Yermak 2007, and 9 from NPEO 2008). Average profiles from the three separate surveys are shown in Figure 2. In applying K06, a constant shear-strain ratio of $R_\omega = 11$ is applied following the observations of *Fer et al*. [2010] to the Yermak Plateau survey, while the values listed in Table 1 are applied to NPEO 2007 and NPEO 2008. Both parameterizations show good agreement with the microstructure-based estimates, both in terms of amplitudes and vertical variability, and certainly well within the known limitations of both K06 and G89. K06 yields slightly lower diffusivities than the G89 approach used by *D'Asaro and Morison* [1992]. The discrepancy between MSS90L and XCP-derived results for NPEO 2007 may be due to the large time (up to 10 h) and spatial (up to 3 km) separations between XCP-MSS pairs. The NPEO 2007 XCP results are calculated from only four profiles, a small sample size that may not be sufficient enough to produce a representative average profile. Furthermore, this difference highlights the role of intermittent mixing processes and strengthens our approach of multistation averaging to be able to draw conclusions on temporal and spatial trends.

5. Results

[25] Comparison of vertical wave number power spectra of horizontal velocity from the 1980s and from NPEO show ranges of up to an order of magnitude between surveys (Figure 3). Values of E_0 and j_*, along with other calculated quantities, for all surveys are shown in Table 1. All surveys show the presence of more vertical modes than the open ocean with all values of the cutoff mode number, j_*, greater than 25 versus $j_* = 6$ for GM. This is consistent with results from AIWEX [*D'Asaro and Morehead*, 1991]. The increased number of vertical modes results in flatter spectra typical midlatitude spectra. The spectral energy level, E_0, varies between surveys with values ranging between 0.05 and 0.2 of GM. Two of the recent NPEO surveys have the highest value of E_0, roughly a fifth of GM and comparable to MIZEX 83 and Polarstern 87. Surveys from the Canada Basin show low E_0, consistent with previous results [*Levine et al*., 1987; *D'Asaro and Morehead*, 1991]. This is highlighted by the AIWEX spectrum and the XCPs dropped from the Louis St. Laurent in 2007 with values of 0.05 and 0.11 of GM, respectively. However, recent central Arctic Ocean surveys, NPEO 2010 and NPEO 2012, show similarly low energy levels, 0.057 and 0.065 of GM, respectively.

[26] Rotary spectral analysis was also performed [*Gonella*, 1972; *Leaman and Sanford*, 1975] to calculate survey-averaged CW versus CCW variance ratio (see Table 1). This can be interpreted as a ratio of downward propagating to upward propagating energy. Values for all surveys range between 1 and 2, indicating a slight net downward internal wave energy propagation. The Louis 2007 cruise has the highest ratio, 1.8. This was a cruise during the summer of a record minimum sea ice extent. It makes sense in terms of enhanced internal wave generation being under reduced ice cover that this value is higher than the other surveys, which were either made during springtime or in the summertime in the presence of more sea ice. Comparison with the historical

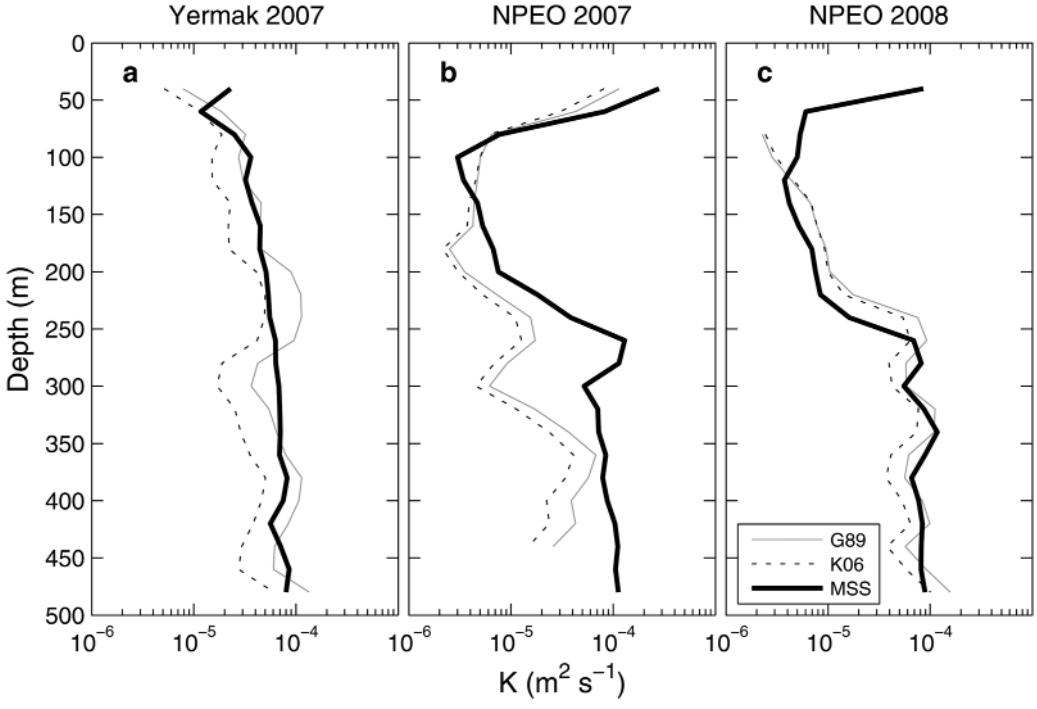

Figure 2. Direct comparison between K parameterized from XCP drops using the *Gregg* [1989] (G89) and *Kunze et al*. [2006] (K06) parameterizations with K estimated from microstructure observations for three surveys. (a) Yermak 2007, (b) NPEO 2007, and (c) NPEO 2008.

Table 1. Calculated Properties[a]

Survey	Date	Number of Profiles	j_*/j_{*GM}	E_0/E_{0GM}	K	R_ω	CW/CCW	Max F_H
Louis 2007	Aug 2007	5	4.7	0.11	5.5×10^{-6}	4	1.83	0.33
NPEO 2007	Apr 2007	7	11	0.07	1.1×10^{-5}	7	1.35	0.22
NPEO 2008	Apr 2008	7	6	0.25	9.5×10^{-6}	6	1.39	0.3
NPEO 2010	Apr 2010	13	7.7	0.06	5.7×10^{-6}	8	1.02	0.15
NPEO 2011	Apr 2011	6	6	0.16	2.5×10^{-5}	11	1.08	1.2
NPEO 2012	Apr 2012	10	8	0.07	5.4×10^{-6}	10	1.21	0.19
MIZEX 83	Jun/Jul 1983	11	5	0.19	1.2×10^{-5}	11	1.03	0.67
Polarstern 87	Jul/Aug 1987	20	6.3	0.11	2×10^{-5}	11	.99	1.58
AIWEX	Mar/Apr 1987	40	7.3	0.05	1.1×10^{-6}	12	1.11	0.09

[a]Values from the results shown for all surveys are listed above.

data (MIZEX 83, Polarstern 87, AIWEX) suggests a very small increase in the amount of downward propagating energy present between 150 and 400 m, but the increase is not statistically significant and a clear temporal trend is hard to justify.

[27] Survey-averaged diffusivity profiles are shown in Figure 4. Diffusivity is typically O[10^{-6} m^2 s^{-1}] in the upper (cold halocline) part of the profile consistent with estimates from *D'Asaro and Morison* [1992] and recent observations [*Fer*, 2009; *Rainville and Winsor*, 2008]. MIZEX 83, Polarstern 87, and NPEO 2011 have higher K, while the two Beaufort Sea surveys (AIWEX and Louis 2007) are the lowest. Below the CHL, diffusivity increases to O[10^{-5} m^2 s^{-1}] and even approaches O[10^{-4} m^2 s^{-1}] in the case of NPEO 2011. While the calculation of K is dependent on R_ω, it is not strongly so. An increase of R_ω from 3 (GM value) to 6 or 12 leads to a factor of 1.8 or 2.9 reduction in K.

[28] Buoyancy Reynolds number or Turbulent Activity Index, $\varepsilon/\nu N^2$, analysis supports the low diffusivities inferred

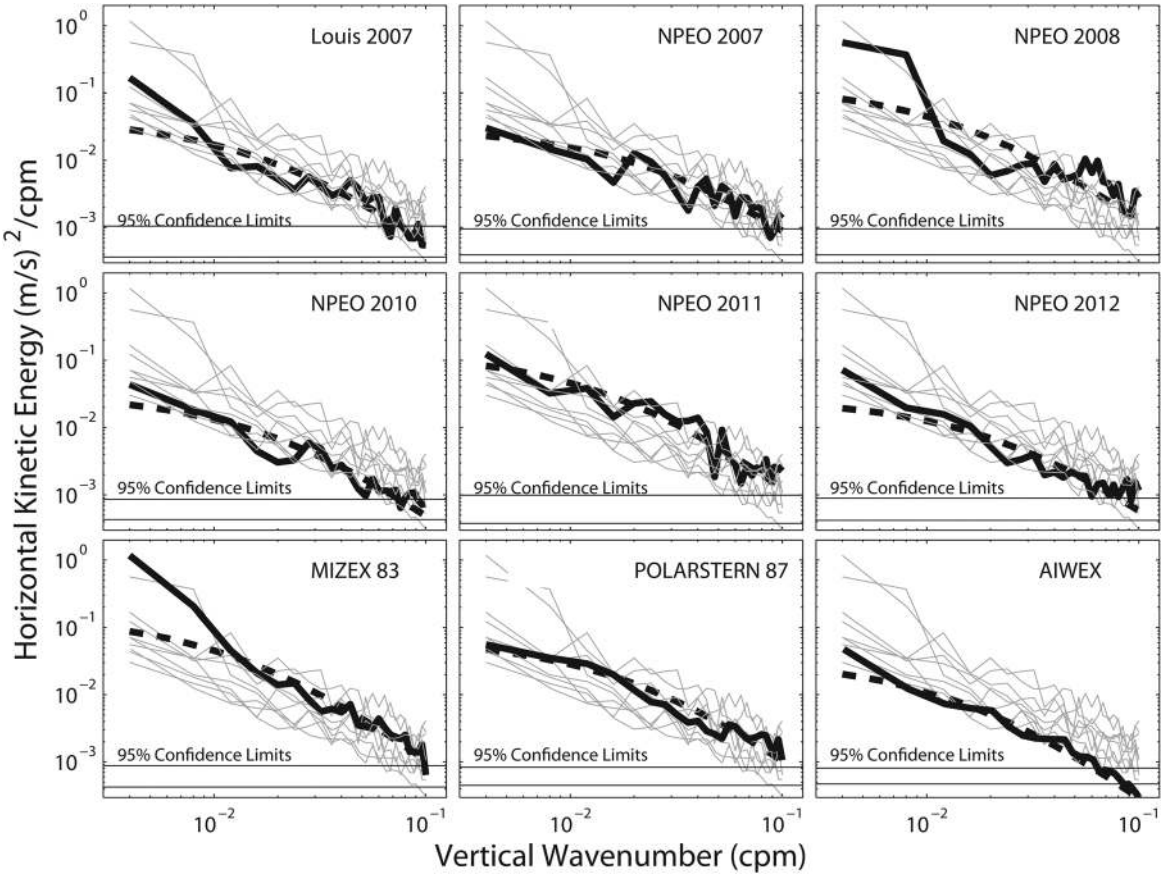

Figure 3. Survey-averaged WKB scaled vertical wave number spectra of horizontal kinetic energy. Survey listed in the title is given in solid black, and a GM fit is given in dashed black. The light grey lines are the other surveys.

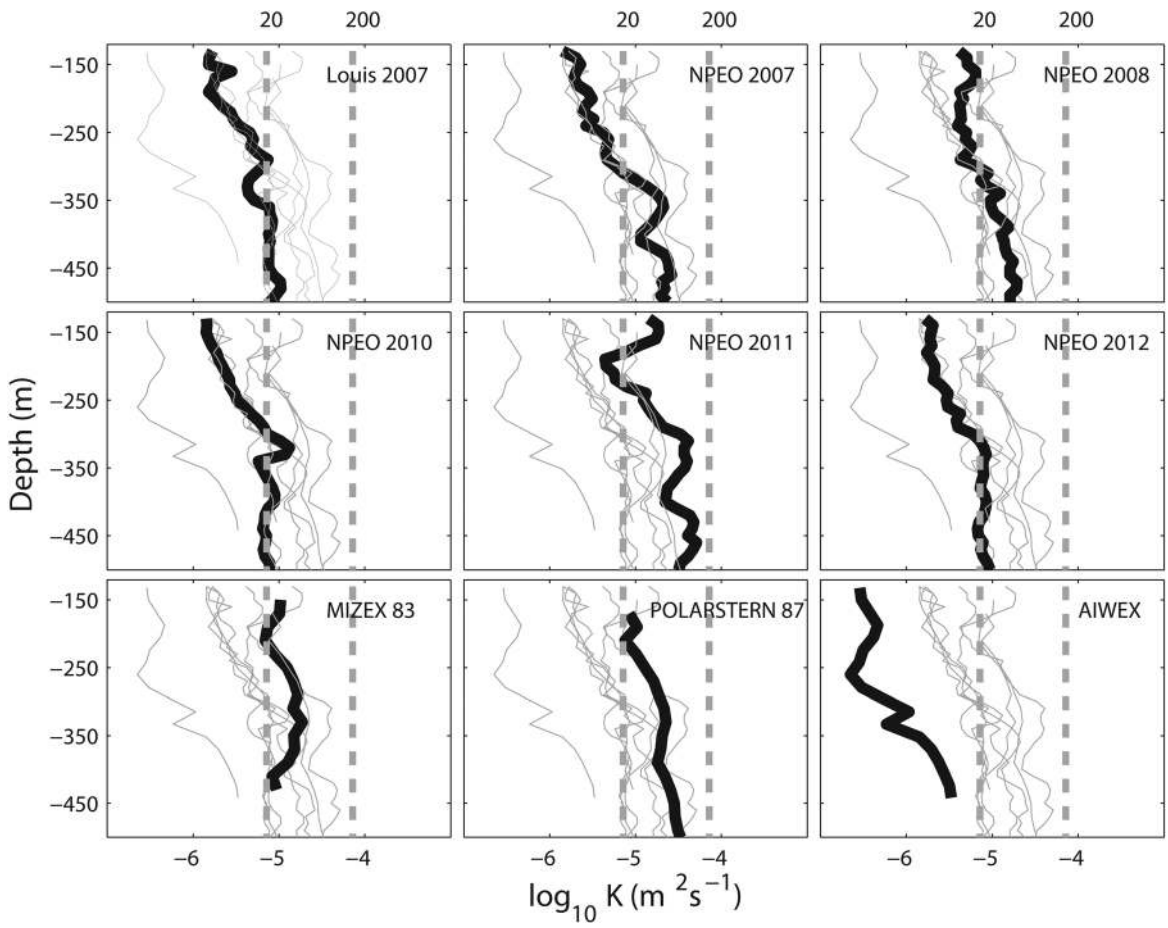

Figure 4. Survey-averaged diffusivity. Survey listed in the legend. Light grey lines are the other surveys. The dashed grey lines represent values of $\varepsilon/\nu N^2 = 20$ and 200, respectively.

from the K06 parameterization. It is a predictor of the efficiency of turbulence in overcoming stratification and producing mixing with $\varepsilon/\nu N^2 \approx 20$ being the minimum value for which turbulent mixing becomes important. Below this value, the turbulence is not strong enough to induce a buoyancy flux [*Gregg and Sanford*, 1988; *Stillinger et al*., 1983]. Across the CHL, this value is below 20 for all surveys except NPEO 2011, Polarstern 87, and MIZEX 83 (see Figure 4). However for most surveys, this value exceeds 20 close to the AW temperature maximum (∼250 m) where stratification weakens. For NPEO 2010, NPEO 2012, and Louis 2007, turbulence might be unimportant at all depth ranges analyzed.

[29] Survey-averaged mean K values between 150 and 400 m for all XCP data sets (Figure 5) show no clear temporal trend. Excluding AIWEX, depth-averaged (150–400 m) diffusivities range from 5×10^{-6} (Louis 2007) to 2×10^{-5} m^2 s^{-1} (NPEO 2011). Calculating depth averages solely across the most stratified part of the cold halocline (e.g., 150–250 m) yields diffusivities of O[10^{-6} m^2 s^{-1}], lower than most oceanic shear microstructure measurements, O[10^{-5} m^2 s^{-1}], but of the same order of magnitude as recent microstructure measurements in the Arctic [*Fer*, 2009; *Rainville and Winsor*, 2008].

[30] Perhaps the most surprising facet of the XCP results is the low diffusivity characterizing the Beaufort Sea region. In the early period, the average AIWEX diffusivity is an order of magnitude lower than MIZEX 83 and Polarstern 87. In the recent data, Louis 2007 and the Beaufort Sea NPEO 2008 profiles yielded diffusivities higher than AIWEX, but they are among the lowest from the recent

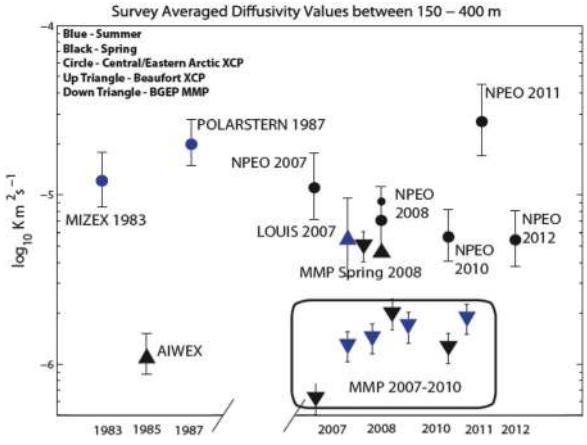

Figure 5. Survey-averaged mean diffusivity between 150 and 400 m. Black icons represent springtime surveys (March/April). Blue icons represent summertime surveys (June/July/August). Circles are central/eastern Arctic XCP data. Upward triangles are Beaufort Sea XCP data. Downward triangles are Beaufort Sea MMP data.

surveys. Louis 2007 and NPEO 2008 (Beaufort) consisted of few profiles resulting in wide confidence limits. The diffusivities from the MMP profiles from 2007 to 2010 are directly comparable. Except for spring 2008, the MMP-derived diffusivities average 1.5×10^{-6} m^2 s^{-1} compared to 1.1×10^{-6} m^2 s^{-1} for AIWEX. Only the spring 2008 gives an MMP-derived diffusivity of 5×10^{-6} m^2 s^{-1} in agreement with the NPEO 2008 (Beaufort) values. To test whether these results were sensitive to our choice of sampling periods (spring and late summer), we also computed month-by-month averages of diffusivities for the 2007–2010 MMP time series. The month-by-month composite diffusivities range only from 1.4×10^{-6} m^2 s^{-1} in April to 3×10^{-6} m^2 s^{-1} in January, the April value well within the error bars for the springtime AIWEX diffusivity.

[31] We have also calculated turbulent heat fluxes using the diffusivities derived here (Figure 6). The most energetic surveys (NPEO 2011, MIZEX 83, Polarstern 87) display F_H ranging between −2 and 2 W m^{-2}. Most of the NPEO 2011 profile is similar to the other NPEO surveys except for large fluxes near 120 m that results from higher diffusivity at that depth. The Polarstern 87 and MIZEX 83 heat fluxes are consistent with those found by *D'Asaro and Morison* [1992]. These are larger than the heat fluxes measured during the other surveys due to the proximity of ARKTIS IV/3 and MIZEX 83 to the warm Atlantic Water inflow to the Arctic Ocean and comparable to the large heat fluxes observed in the boundary current on the East Siberian continental slope [*Lenn et al.*, 2009]. The values of F_H from the NPEO data (except 2011), AIWEX, and Louis 2007 vary between −0.3 and 0.3 W m^{-2}, similar to double-diffusive estimates from both Ice-Tethered Profiler (ITP) [*Timmermans et al.*, 2008] and microstructure [*Sirevaag and Fer*, 2012] measurements. The NPEO surveys suggest that temperature gradient is still the controlling factor in this calculation as the diffusivities differed significantly in some areas, yet outside the depths of elevated diffusivities found in the NPEO 2011 profile; the heat flux profiles are remarkably consistent from year to year.

6. Discussion

[32] In the Arctic Ocean, internal wave energy varies significantly, but all surveys show less energy than typical midlatitude GM values and much broader bandwidth. Diffusivities in the Beaufort Sea measured recently and decades in the past show levels at the bottom of the range. Parameterized mixing values across the cold halocline are lower, O[10^{-6} m^2 s^{-1}] than typical open ocean values measured by microstructure O[10^{-5} m^2 s^{-1}]. However, most surveys begin to increase toward this value at around 300 m depth. Values of parameterized ε remain low (below the noise level of most previous microstructure measurements) across all depth ranges analyzed, and the increasing diffusivities with depth result from the decreasing stratification.

[33] There is also a question of whether the latitudinal dependence term, $L(f,N)$ (equation (3)) is applicable in this study, but our diffusivity estimates are not low because of it. This correction is an empirical result but has only been verified in midlatitudes [*Gregg et al.*, 2003]. The large f (1.45×10^{-4} s^{-1}) found at high latitudes could lead to an overestimation of K, as $L(f,N)$ can effectively double the diffusivity at high latitudes in the presence of strong stratification, such as across the CHL. Our inclusion of this correction should be conservative with respect to inferring that diffusivities are low.

[34] Our results suggest that the amount of open water and strength of the ice are not the dominant factors

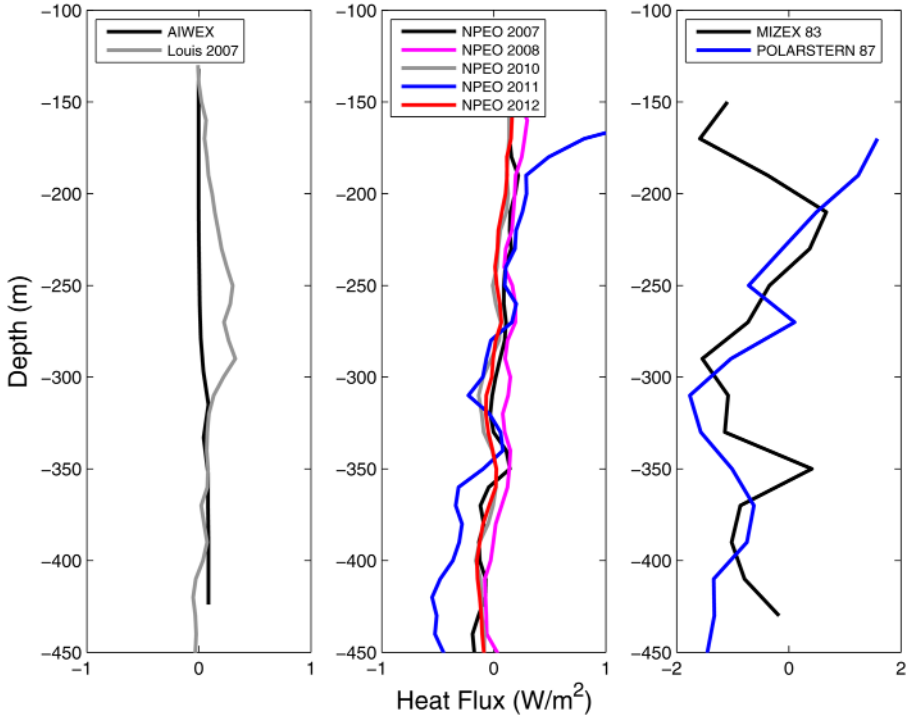

Figure 6. Values of turbulent heat flux calculated for all XCP surveys.

responsible for determining internal wave energy and mixing. The more recent estimates of diffusivity in the Beaufort Sea (Louis 2007 and three profiles from NPEO 2008) are somewhat higher than the values from AIWEX. Values from summertime when ice is thin and free to move (Louis 2007) and from springtime when ice is thicker and more compact (NPEO 2008) are similar. Analysis of the MMP data from 2007 to 2010 reveals that although the spring of 2008 shows the highest diffusivities, typical diffusivities in spring are either less than or of the same magnitude as those in summer (see inset Figure 5). This whole period comes immediately after the 2007 Arctic sea ice minimum and significant increases in the freshwater content of the Beaufort Sea [*McPhee et al*., 2009; *Morison et al*., 2012; *Proshutinsky et al*., 2009].

[35] In the presence of an ice cover, internal wave energy and background mixing may be most sensitive to upper ocean stratification. Internal wave energies and the consequent deep background mixing are about a factor of 5 lower in the Beaufort Sea than in the central Arctic Ocean. These regions should have similar internal wave forcing; indeed we might expect stronger forcing in the Beaufort Sea region where record reductions in the sea ice have occurred. For the Beaufort Sea, the effect of stronger near-surface stratification (Figure 7a) on internal wave dissipation in the boundary layer immediately under sea presents a possible explanation for persistently low internal wave energies and mixing.

[36] Internal wave energy is dissipated in oscillating boundary layers under sea ice, and this process limits steady state internal wave energy [*Morison et al*., 1985; *Pinkel*, 2005]. As illustrated in the schematic of Figures 8a and 8b, the surface boundary condition for internal wave horizontal velocity is free in open water, but under ice a no-slip boundary condition applies. The influence of the no-slip boundary condition imposed by the ice on internal wave velocities increases with degree of stratification below the mixed layer. Considering the normal modes of internal waves, the velocity corresponding to each mode just outside the under-ice boundary layer (e.g., at the base of the mixed layer) is proportional to the vertical derivative of the corresponding displacement mode shape. This is illustrated in crude fashion by comparing the first mode behavior in a two-layer ocean with deep (Figure 8b) and shallow (Figure 8c) upper layers. If near-surface stratification is increased, due either to freshening or shoaling of the mixed layer, the horizontal velocity associated with each mode is increased relative to the velocity at greater depth. For a given internal wave energy at depth, an increase in near-surface stratification will result in greater internal wave horizontal velocity approaching the surface and greater dissipation in the turbulent under-ice boundary layer. This being the case, we should expect to see perpetually lower internal wave energy in the Beaufort Sea where near-surface stratification is greater than in the Nansen and Amundsen basins (Figure 7a). Other things being equal, we might also expect internal wave energy and mixing to decrease after a major surface freshening as occurred in 2007–2008. Dominance of under-ice boundary layer dissipation in Arctic internal wave dynamics may account for the negative correlation, $r = -0.59$ significant at the 0.05 level, between XCP survey average mixing and near-surface stratification (Figure 7b). The MMP record from summer 2007 indicates that the diffusivity estimated by the Louis 2007 XCPs is anomalously high. Removing the mean diffusivity value of the Louis 2007 data strengthens the negative correlation of diffusivity with stratification to $r = -0.71$.

[37] We explore the influence of stratification and boundary layer dissipation on internal wave energy by extrapolating on the results of *Morison et al*. [1985]. To estimate the dissipation of internal wave energy in the boundary layer imposed by the no-slip condition at the ice-water interface, *Morison et al*. [1985] drove an oscillating boundary layer model [*Long*, 1981] with a discrete spectrum of horizontal velocities representing free-stream internal wave horizontal

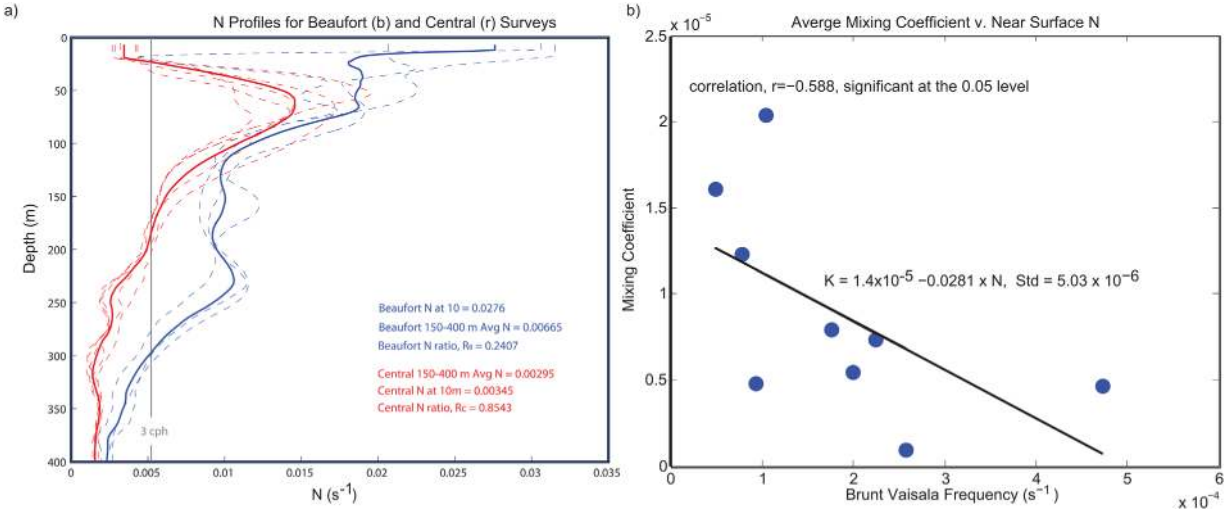

Figure 7. Comparisons of XCP survey stratification and mixing coefficients (a) Brunt-Väisälä frequency, *N*, profiles versus depth for XCP for Beaufort and central Arctic Ocean surveys and average regional *N* profiles (thick lines). (b) XCP-survey-averaged mixing coefficients plotted versus survey-averaged *N* in the upper part of the ocean.

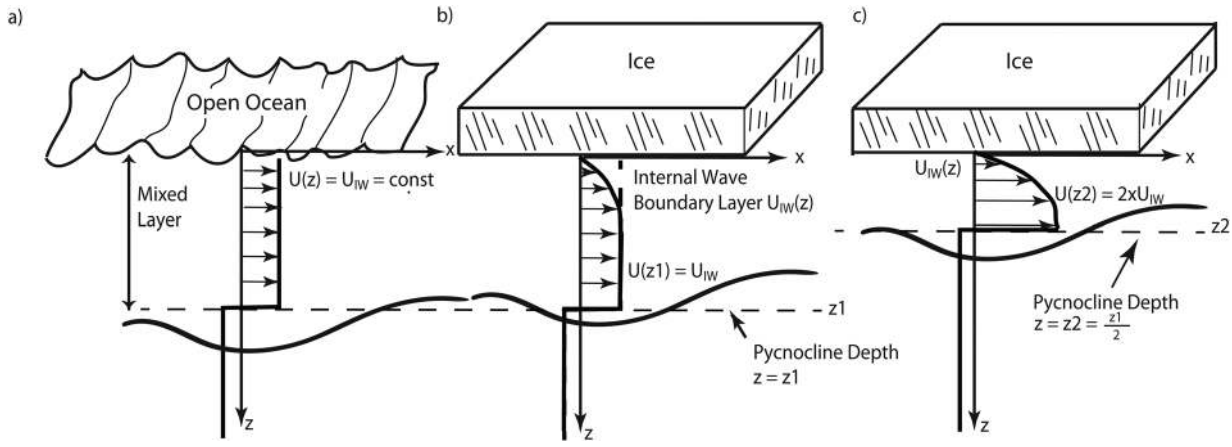

Figure 8. Schematic (adapted from *Morison et al*. [1985]) illustrating the difference in internal wave boundary conditions between (a) the open ocean, (b) an ice covered ocean, and (c) an ice covered ocean with increased near-surface stratification idealized as a reduction in upper layer depth and consequent increase in the first internal wave mode upper layer velocity.

velocities near the surface. These were derived from observations of vertical displacement at 50 to 150 m depth at the Fram III ice camp north of the Yermak Plateau in 1981 [*Levine et al*., 1985]. The *Desaubies* [1976] formulation of the GM model was used to parameterize the displacement and velocity spectra at Fram III using N equal to 3 cph (0.0052 s^{-1}) and a magnitude about one sixth of GM. The interaction of the internal waves with the boundary layer was linearized by assuming that the turbulence level was dominated by the RMS velocity of the ice, $U_{ice} = 7$ cm s^{-1}, with the consequence that the boundary layer dissipation of internal wave energy, Q_{bl}, is proportional to $U_{ice}U_w^2$, where U_w^2 is the internal wave energy just outside the oscillating under-ice boundary layer. Approximating the total internal wave energy with a first-order differential equation, they found that the corresponding time scale for internal wave dissipation is $\tau_{bl} = 32$ days, one third that for open ocean conditions, $\tau_{ow} = 100$ days [*Olbers*, 1983] without an internal wave boundary layer. Assuming equal forcing, the ratio of internal wave energy in the under-ice environment to the open ocean internal wave energy is $E_{IC}/E_{OW} = \tau_{BL}(\tau_{BL} + \tau_{OW})^{-1} = 0.24$ indicating a factor of 4 reduction in energy relative to open ocean conditions due solely to boundary layer dissipation.

[38] The impact of near-surface stratification on the rate of internal dissipation in the under-ice boundary layer is a fundamental outcome of WKB scaling [*Leaman and Sanford*, 1975]. *Morison et al*. [1985] used internal wave measurements near the surface to drive their model and thus did not consider the variation of internal wave horizontal velocity with stratification. As long as stratification near the surface is not too different from that at depth (e.g., central Arctic Ocean N profile in Figure 7a), variations in N are probably not critical to the boundary layer dissipation calculation, but in cases where N is dramatically higher in the upper part of the halocline, as in the Beaufort Sea (Figure 7a), WKB scaling, $U_w \sim N^{1/2}$, [*Leaman and Sanford*, 1975] suggests U_w^2 will be amplified relative to the internal wave energy in the rest of the water column. This should result in enhanced boundary layer dissipation and a boundary dissipation time scale shortened by a factor of R, the ratio of N deep in the water column to N near the base of the boundary layer. Considering two under-ice locations, B and C, with similar forcing, but markedly different N profiles such as the Beaufort Sea and central Arctic Ocean, the difference in energies due to the difference in stratification would be $\frac{E_B}{E_C} = \frac{R_B(R_C\tau_{BL}+\tau_{OW})}{R_C(R_B\tau_{BL}+\tau_{OW})}$, where R_B and R_C are the N ratios at B and C, respectively. Taking B to represent the Beaufort Sea and comparing N from 150 to 400 m to N at 10 m, we find $R_B = 0.24$ (Figure 7a). Letting C represent the central Arctic Ocean, $R_C = 0.85$. Thus, we expect that, owing only to boundary layer dissipation, internal wave energy and mixing in the Beaufort Sea to be a factor of 0.333 times the energy and mixing in the central Arctic Ocean. The enhanced dissipation due to higher near-surface stratification in the Beaufort Sea could be responsible for a major fraction of the observed difference in internal wave energies between the basins.

[39] Our argument does not include the effects of increasing ice velocity. If the typical RMS ice velocity increases because the ice is weaker, we might expect the dissipation of internal wave energy in the boundary layer to increase and tend to reduce internal wave energy. If the ice moves faster because the ice is thinner and smoother we might expect a corresponding reduction on the ice-water drag coefficient and the effect on internal wave energies would be negligible. In any case, our observations suggest that in the presence of sea ice, boundary layer damping keeps internal wave energies and mixing low in spite of possible enhanced forcing due to increased ice mobility.

[40] The average effect of boundary layer dissipation should decrease proportional to increases in the fraction of open water. This effect, along with enhanced ice motion, may overshadow the increase in under-ice boundary layer damping due summertime increases in stratification in the Beaufort Sea, where MMP-derived summer diffusivities are commonly, although not always, a little higher than wintertime diffusivities.

[41] We add a cautionary note about stratification near the surface. The boundary layer model of *Morison et al*. [1985] assumes an unstratified boundary layer; a mixed

layer of at least a few meters under the ice is required. If strong stratification extends to the very bottom of the ice, we might expect boundary layer stress and dissipation to decrease in the stable boundary layer, opening the way for temporary increases in internal energy. A more complete approach would allow for the effect of buoyancy flux [*Fer and Sundfjord*, 2007; *Perlin et al*., 2005] in the oscillating boundary layer model.

[42] Finally, our dissipation values across the halocline fall within the upper bound of turbulent dissipation presented in *Timmermans et al*. [2008] based on measurements made by *Halle and Pinkel* [2003] in the Canada Basin during the Sea Ice Mechanics Initiative (SIMI) experiment. *Timmermans et al*. [2008] took the *Halle and Pinkel* [2003] calculated downward internal wave energy fluxes and assumed that all of the energy was dissipated in the halocline. By assuming that stratification across the halocline averages 4×10^{-5} s^{-2} and that a typical CHL depth was 100 m, the measured internal wave energy flux of 0.15 mW m^{-2} would result in a diffusivity of 5×10^{-6} m^2 s^{-1}. This is an upper bound because it requires all the energy to dissipate in the CHL, which is unlikely. Expanding the argument presented in *Timmermans et al*. [2008] and assuming average Arctic Ocean temperature gradients from our data (0.01°C m^{-1} in the Beaufort Sea and 0.0133°C m^{-1} in the central Arctic Ocean) and the same CHL depths and stratification, we find that diffusivities in the central Arctic Ocean across the CHL would have to reach 3.7×10^{-5} m^2 s^{-1} for heat fluxes away from topography to reach 2 W m^{-2}, the value required by *Maykut and Untersteiner* [1971] for oceanic heat to negatively affect sea ice concentration from the current thermodynamic balance. In the Beaufort Sea, diffusivity would have to be even higher to reach 2 W m^{-2}, given the less steep temperature gradients in that basin. Melting the ice from underneath in the central Arctic Ocean due to increased vertical mixing from the AW layer would require downward internal wave energy fluxes roughly 5 times as high (0.75 mW m^{-2}) as those measured by *Halle and Pinkel* [2003] during a strong storm event in the Beaufort Sea. Based on current measurements, it seems unlikely that heat fluxes of this magnitude across the CHL will happen in the near-future without drastic changes in both surface forcing and temperature gradients. Increasing K in the Arctic Ocean to typical open ocean thermocline levels, 10^{-5} m^2 s^{-1}, only results in heat fluxes ranging between 0.4 and 0.55 W m^{-2}, slightly higher than double diffusive estimates [*Sirevaag and Fer*, 2012; *Timmermans et al*., 2008].

[43] **Acknowledgments.** This work has been supported by NSF grants ARC-0909408 and ARC-0856330 and the Research Council of Norway through project 196161. Thanks to Eric D'Asaro for recovering and providing the data from *D'Asaro and Morison* [1992]. The Louis 2007 XCP and MMP data were kindly collected by the Beaufort Gyre Exploration Program (BGEP) based at the Woods Hole Oceanographic Institution (http://www.whoi.edu/beaufortgyre) in collaboration with researchers from Fisheries and Oceans Canada at the Institute of Ocean Sciences.

References

D'Asaro, E. A., and M. Morehead (1991), Internal waves and velocity fine structure in the Arctic Ocean, *J. Geophys. Res.*, *96*(C7), 12,725–12,738, doi:10.1029/91JC01071.

D'Asaro, E. A., and J. H. Morison (1992), Internal waves and mixing in the Arctic Ocean, *Deep Sea Res., Part A*, *39*, suppl. 2, S459–S484.

Desaubies, Y. J. F. (1976), Analytical representation of internal wave spectra, *J. Phys. Oceanogr.*, *6*(6), 976–981.

Fer, I. (2006), Scaling turbulent dissipation in an Arctic fjord, *Deep Sea Res. II*, *53*(1-2), 77–95.

Fer, I. (2009), Weak vertical diffusion allows maintenance of cold halocline in the central Arctic, *Atmos. Ocean. Sci. Lett.*, *2*(3), 148–152.

Fer, I., and A. Sundfjord (2007), Observations of upper ocean boundary layer dynamics in the marginal ice zone, *J. Geophys. Res.*, *112*, C04012, doi:10.1029/2005JC003428.

Fer, I., R. Skogseth, F. Geyer (2010), Internal Waves and Mixing in the Marginal Ice Zone near the Yermak Plateau, *J. Phys. Oceanogr.*, *40*, 1613–1630, doi:10.1175/2010JPO4371.1.

Fofonoff, N. P. (1985), Physical properties of seawater: A new salinity scale and equation of state for seawater, *J. Geophys. Res.*, *90*(C2), 3332–3342, doi:10.1029/JC090iC02p03332.

Garrett, C. J., and W. H. Munk (1972), Space-time scales of internal waves, *Geophys. Fluid Dyn.*, *2*, 225–264.

Garrett, C. J., and W. H. Munk (1975), Space-time scales of internal waves: A progress report, *J. Geophys. Res.*, *80*(3), 291–297, doi:10.1029/JC080i003p00291.

Gonella, J. (1972), A rotary-component method for analyzing meteorological and oceanographic vector time series, *Deep Sea Res. Oceanogr. Abstr.*, *19*, 833–846.

Gregg, M. C. (1989), Scaling turbulent dissipation in the thermocline, *J. Geophys. Res.*, *94*(C7), 9686–9698, doi:10.1029/JC094iC07p09686.

Gregg, M. C., and T. B. Sanford (1988), The dependence of turbulent dissipation on stratification in a diffusively stable thermocline, *J. Geophys. Res.*, *93*(C10), 12,381–12,392, doi:10.1029/JC093iC10p12381.

Gregg, M. C., T. B. Sanford, and D. P. Winkel (2003), Reduced mixing from the breaking of internal waves in equatorial waters, *Nature*, *422*, 513–515.

Halle, C., and R. Pinkel (2003), Internal wave variability in the Beaufort Sea during the winter of 1993/1994, *J. Geophys. Res.*, *108*(C7), 3210, doi:10.1029/2000JC000703.

Kunze, E., E. Firing, J. M. Hummon, T. K. Chereskin, and A. M. Thurnherr (2006), Global abyssal mixing inferred from lowered ADCP shear and CTD strain profiles, *J. Phys. Oceangr.*, *36*(12), 2350–2352.

Kwok, R., G. F. Cunningham, M. Wesnahan, I. Rigor, H. J. Swally, and D. Yi (2009), Thinning and volume loss of the Arctic Ocean sea ice cover: 2003–2008, *J. Geophys. Res.*, *114*, C07005, doi:10.1029/2009JC005312.

Large, W. G., J. C. McWilliams, and S. C. Doney (1994), Oceanic vertical mixing—A review and a model with a nonlocal boundary-layer parameterization, *Rev. Geophys.*, *32*(4), 363–403.

Leaman, K. D., and T. B. Sanford (1975), Vertical energy propagation of inertial waves: A vector spectral analysis of velocity profiles, *J. Geophys. Res.*, *80*(15), 1975–1978, doi:10.1029/JC080i015p01975.

Lee, C. M., E. Kunze, T. B. Sanford, J. D. Nash, M. A. Merrifield, and P. E. Holloway (2006), Internal tides and turbulence along the 3000-m isobath of the Hawaiian Ridge, *J. Phys. Oceanogr.*, *36*, 1165–1183.

Lenn, Y. D., et al. (2009), Vertical mixing at intermediate depths in the Arctic boundary current, *Geophys. Res. Lett.*, *36*, L05601, doi:10.1029/2008GL036792.

Levine, M. D., C. A. Paulson, and J. H. Morison (1985), Internal waves in the Arctic Ocean—Comparison with lower-latitude observations, *J. Phys. Oceanogr.*, *15*(6), 800–809.

Levine, M. D., C. A. Paulson, and J. H. Morison (1987), Observations of internal gravity-waves under the Arctic Pack Ice, *J. Geophys. Res.*, *92*(C1), 779–782, doi:10.1029/JC092iC01p00779.

Long, C. E. (1981), *A Simple Model for Time-Dependent Stably Stratified Turbulent Boundary Layers*, Univ. of Washington, Seattle.

Maykut, G. A., and N. Untersteiner (1971), Some results from a time-dependent thermodynamic model of sea ice, *J. Geophys. Res.*, *76*(6), 1550–1575, doi:10.1029/JC076i006p01550.

McPhee, M. G. (2008), *Air-Ice-Ocean Interaction: Turbulent Ocean Boundary Layer Exchange Processes*, Springer, N. Y.

McPhee, M. G., A. Proshutinsky, J. Morison, M. Steele, and M. Alkire (2009), Rapid change in freshwater content of the Arctic Ocean, *Geophys. Res. Lett.*, *36*, L10602, doi:10.1029/2009GL037525.

Merrifield, M., and R. Pinkel (1996), Inertial currents in the Beaufort Sea: Observations of response to wind and shear, *J. Geophys. Res.*, *101*(C3), 6577–6590, doi:10.1029/95JC03625.

Morison, J., C. E. Long, and M. D. Levine (1985), The dissipation of internal wave energy under arctic ice, *J. Geophys. Res.*, *90*(C6), 11,959–11,966.

Morison, J., R. Kwok, C. Peralta-Ferriz, M. Alkire, I. Rigor, R. Andersen, and M. Steele (2012), Changing Arctic Ocean freshwater pathways, *Nature*, *481*(7379), 66–70.

Munk, W. (1966), Abyssal recipes, *Deep Sea Res. Oceanogr. Abstr.*, *13*, 707–730.

Munk, W., and C. Wunsch (1998), Abyssal recipes: II. Energetics of tidal and wind mixing, *Deep Sea Res., Part I*, *45*(12), 1977–2010.

Nash, J. D., M. H. Alford, E. Kunze, K. Martini, and S. Kelly (2007), Hotspots of deep ocean mixing on the Oregon continental slope, *Geophys. Res. Lett.*, *34*, L01605, doi:10.1029/2006GL028170.

Olbers, D. J. (1983), Models of the oceanic internal wave fields, *Rev. Geophys.*, *21*(7), 1567–1606.

Osborn, T. R. (1980), Estimates of the local rate of diffusion from dissipation measurements, *J. Phys. Oceanogr.*, *10*, 83–89.

Padman, L., and T. M. Dillon (1991), Turbulent mixing near the Yermak Plateau during the Coordinated Eastern Arctic Experiment, *J. Geophys. Res.*, *96*(C3), 4769–4782, doi:10.1029/90JC02260.

Padman, L., M. Levine, T. Dillon, J. Morison, and R. Pinkel (1990), Hydrography and microstructure of an Arctic cyclonic eddy, *J. Geophys. Res.*, *95*(C6), 9411–9420, doi:10.1029/JC095iC06p09411.

Perlin, A., J. N. Moum, J. M. Klymak, M. D. Levine, T. Boyd, and P. M. Kosro (2005), A modified law-of-the-wall applied to oceanic bottom boundary layers, *J. Geophys. Res.*, *110*, C10S10, doi:10.1029/2004JC002310.

Pinkel, R. (2005), Near-inertial wave propagation in the western Arctic, *J. Phys. Oceanogr.*, *35*(5), 645–665.

Plueddemann, A. J., R. Krishfield, T. Takizawa, K. Hatakeyama, and S. Honjo (1998), Upper ocean velocities in the Beaufort Gyre, *Geophys. Res. Lett.*, *25*(2), 183–186, doi:10.1029/97GL53638.

Polyakov, I. V., J. E. Walsh, and R. Kwok (2011), Recent changes of Arctic multiyear sea ice coverage and the likely causes, *Bull. Am. Meteorol. Soc.*, *93*(2), 145–151.

Polzin, K. L., J. M. Toole, and R. W. Schmitt (1995), Finescale parameterizations of turbulent dissipation, *J. Phys. Oceanogr.*, *25*, 306–328.

Proshutinsky, A., R. Krishfield, M. L. Timmermans, J. Toole, E. Carmack, F. McLaughlin, W. J. Williams, S. Zimmermann, M. Itoh, and K. Shimada (2009), Beaufort Gyre freshwater reservoir: State and variability from observations, *J. Geophys. Res.*, *114*, C00A10, doi:10.1029/2008JC005104.

Rainville, L., and P. Winsor (2008), Mixing across the Arctic Ocean: Microstructure observations during the Beringia 2005 Expedition, *Geophys. Res. Lett.*, *35*, L08606, doi:10.1029/2008GL033532.

Rainville, L., and R. A. Woodgate (2009), Observations of internal wave generation in the seasonally ice-free Arctic, *Geophys. Res. Lett.*, *36*, L23604, doi:10.1029/2009GL041291.

Rothrock, D. A., D. B. Percival, and M. Wensnahan (2008), The decline in arctic sea-ice thickness: Separating the spatial, annual, and interannual variability in a quarter century of submarine data, *J. Geophys. Res.*, *113*, C05003, doi:10.1029/2007JC004252.

Simmons, H. L., R. W. Hallberg, and B. K. Arbic (2004), Internal wave generation in a global baroclinic tide model, *Deep Sea Res., Part II*, *51*, 3043–3068.

Sirevaag, A., and I. Fer (2012), Vertical heat transfer in the Arctic Ocean: The role of double-diffusive mixing, *J. Geophys. Res.*, *117*, C07010, doi:10.1029/2012JC007910.

St. Laurent, L. C., H. L. Simmons, and S. R. Jayne (2002), Estimating tidally driven mixing in the deep ocean, *Geophys. Res. Lett.*, *29*(23), 2106, doi:10.1029/2002GL015633.

Steele, M., and T. Boyd (1998), Retreat of the cold halocline layer in the Arctic Ocean, *J. Geophys. Res.*, *103*(C5), 10,419–10,435, doi:10.1029/98JC00580.

Steele, M., R. Morley, and W. Ermold (2001), PHC: A global ocean hydrography with a high-quality Arctic Ocean, *J. Clim.*, *14*(9), 2079–2087.

Stillinger, D. C., K. N. Helland, and C. W. V. Atta (1983), Experiments on the transition of homogeneous turbulence to internal waves in a stratified fluid, *J. Fluid Mech.*, *131*, 91–122.

Stroeve, J., M. M. Holland, W. Meier, T. Scambos, and M. Serreze (2007), Arctic sea ice decline: Faster than forecast, *Geophys. Res. Lett.*, *34*, L09501, doi:10.1029/2007GL029703.

Timmermans, M. L., J. Toole, R. Krishfield, and P. Winsor (2008), Ice-Tethered Profiler observations of the double-diffusive staircase in the Canada Basin thermocline, *J. Geophys. Res.*, *113*, C00A02, doi:10.1029/2008JC004829.

Zhang, J. L., and M. Steele (2007), Effect of vertical mixing on the Atlantic Water layer circulation in the Arctic Ocean, *J. Geophys. Res.*, *112*, C04S04, doi:10.1029/2006JC003732.